HHS Public Access

Author manuscript

*Dev Neurobiol*. Author manuscript; available in PMC 2019 June 01.

Published in final edited form as:

*Dev Neurobiol*. 2018 June ; 78(6): 627–644. doi:10.1002/dneu.22572.

# Cerebellar microglia are dynamically unique and survey Purkinje neurons *in vivo*

**Rianne D. Stowell**[1], **Elissa L. Wong**[2], **Hanna N. Batchelor**[1], **Monique S. Mendes**[1], **Cassandra E. Lamantia**[1], **Brendan S. Whitelaw**[1], and **Ania K. Majewska**[1,*]

[1]Department of Neuroscience, University of Rochester Medical Center, Rochester, NY, United States

[2]Department of Environmental Medicine, University of Rochester Medical Center, Rochester, NY, United States

## Abstract

Microglia are the innate immune cells of the central nervous system and are also important participants in normal development and synaptic plasticity. Here we demonstrate that the microglia of the mouse cerebellum represent a unique population compared to cortical microglia. Microglia are more sparsely distributed within the cerebellum and have a markedly less ramified morphology compared to their cortical counterparts. Using time-lapse *in vivo* imaging, we found that these differences in distribution and morphology ultimately lead to decreased parenchymal surveillance by cerebellar microglia. We also observed a novel form of somal motility in cerebellar microglia *in vivo*, which has not been described in cortical populations. We captured microglial interactions with Purkinje neurons *in vivo*. Cerebellar microglia interact dynamically with both the dendritic arbors and somas of Purkinje neurons. These findings suggest that cerebellar microglia are physiologically distinct from cortical populations and that these differences may ultimately alter how they could contribute to plasticity and disease processes in the cerebellum.

### Keywords

Microglia; cerebellum; Purkinje neurons; two-photon imaging; motility

## INTRODUCTION

As the resident immune cells of the central nervous system (CNS), microglia are acutely sensitive to homeostatic perturbations, making them vital participants in CNS disease processes and injury resolution. Historically, microglia were considered inert or inactive in the absence of CNS pathology. However, recent studies have demonstrated a critical and dynamic role for microglia during physiological brain function. In the absence of injury or disease, microglia are highly ramified with highly motile processes that rapidly survey the CNS parenchyma (Davalos et al., 2005; Hanisch and Kettenmann, 2007; Nimmerjahn et al., 2005). Multiple *in vivo* studies have demonstrated that microglial process motility enables

*Correspondence: Ania Majewska, University of Rochester Medical Center, 601 Elmwood Avenue, Box 603, Rochester, New York 14642, (585) 275-4173, Fax: (585) 756-5334, ania_majewska@urmc.rochester.edu.

microglia to contact neuronal elements and that changes in neural activity impact microglial process interactions with synapses (Miyamoto et al., 2016; Tremblay et al., 2010; Wake et al., 2009). While the function of these microglia-synapse contacts remains unclear, it has been postulated that these interactions impact structural and functional synaptic remodeling through physical contact and the release of molecules such as growth factors that could impact plasticity and neuronal homeostasis (Parkhurst et al., 2013; Schafer et al., 2012; Sipe et al., 2016). Indeed, during development microglia drive important changes in neuronal circuits through fractalkine, purinergic, and complement signaling which impact the removal of synapses through phagocytosis (Hoshiko et al., 2012; Pagani et al., 2015; Paolicelli et al., 2011; Schafer et al., 2012; Sipe et al., 2016; Stevens et al., 2007; Zhan et al., 2014). From these studies it has become apparent that microglia are critical participants in neuronal plasticity.

While much has been learned about the role of microglia in the healthy brain, current work has concentrated largely on visual and somatosensory cortices, the hippocampus, and the retinogeniculate system. Comparatively little has been done in the cerebellum (Cb) to discern the behavior of physiological cerebellar microglia, with most studies focusing on early development and disease models (Ashwell, 1990; Cardoso et al., 2015; Drew et al., 2015; Kane et al., 2011; Marin-Teva et al., 2004). From these studies it appears that microglia are intimately involved in regulating the survival of Purkinje and granule cells during the developmental time period of neuronal apoptosis and during pathological events such as exposure to alcohol, toxins or infection. However, the dynamic behavior of microglia in the adult Cb has not been studied.

There are a number of reasons to expect that cerebellar microglia may behave differently from those in the thalamus, neocortex and hippocampus. Recent studies have shown that isolated murine microglia from the cerebellum have a higher expression of immunological genes compared to other brain regions. This differential expression increases with age, suggesting that these cells may have a distinct transcriptome and distinct roles (Grabert et al., 2016; Tay et al., 2017). Additionally, microglia of the Cb turn over more rapidly than cortical microglia, which may contribute to their higher sensitivity to homeostatic disruptions during disease and injury (Tay et al., 2017). These recent findings suggest that cerebellar microglia may be a unique population with unique immunological responsiveness.

To date no studies have evaluated microglial dynamics *in vivo* in the Cb and until recently, few studies have attempted to image any feature of the Cb *in vivo* due to the technical difficulties of accessing this area. Here we develop a chronic craniotomy-window preparation that allows for chronic *in vivo* two-photon imaging of transgenic mice with fluorescently labeled microglia and Purkinje neurons. Using this novel technique, in combination with fixed brain tissue analysis, we characterized cerebellar microglia and their interactions and distribution in relation to Purkinje neurons. We demonstrate that in the intact Cb, microglia are sparse and de-ramified, displaying morphological and dynamic profiles that are distinct from cortical microglia. Similar to cortical microglia, cerebellar microglia make dynamic contacts with Purkinje neuron dendrites and somas, and respond rapidly to focal laser injury. In the future it will be important to determine how the unique

properties of cerebellar microglia affect microglial behavior in the context of cerebellar function in health and disease.

## METHODS

### Animals

All experimental protocols were performed in strict accordance with the University of Rochester Committee on Animal Resources and National Institutes of Health Guidelines. Adult mice were bred on a C57BL/6 background in house. CX3CR1-GFP (JAX: 005582) heterozygous mice were used to visualize microglia for fixed tissue analysis and *in vivo* two-photon imaging. CX3CR1-GFP mice were also bred to Ai9 (tdTomato JAX: 007909) and L7cre (JAX: 004146) mice to generate mice (Ai9/L7Cre+/CX3CR1-GFP) where microglia were labeled with GFP and Purkinje neurons were selectively labeled with tdTomato. These mice were either heterozygous or homozygous for Ai9 and L7cre and were also used for *in vivo* imaging and fixed tissue analysis of microglial density and morphology. All mice were genotyped utilizing the JAX protocols for the strains listed. Both male and female mice were used in all the experiments and no sex-specific trends were observed.

### Fixed Tissue Preparation

For analysis of microglial morphology and density within fixed sections of visual cortex (V1) and Cb brain sections, animals were euthanized with an overdose of sodium pentobarbital (Euthasol, Virbac) and transcardially perfused with 0.1M phosphate buffer saline (PBS, pH 7.4) at room temperature (RT) followed by ice cold 4% paraformaldehyde (PFA). Brains were post-fixed in 4% PFA for 4–5 hours at 4°C and then cryoprotected in a 30% sucrose 0.2M phosphate buffer (PB) solution (pH 7.4). 50μm coronal sections were cut on a freezing microtome (Microm; Global Medical Instrumentation) and kept in cryoprotectant (25% 0.2PB, 25% glycerol, 30% ethylene glycol, 20% dd$H_2O$) at 4°C. Approximately three days later, select sections containing V1 and Cb were briefly washed in 0.1M PB (RT), mounted on slides (VWR) and coverslipped using Prolong Gold mounting medium with DAPI (Molecular Probes, P36935).

### Histology

To confirm Iba-1 co-labeling with GFP expression in CX3CR1-GFP mice, V1 and Cb coronal sections underwent Iba-1 immunohistochemistry as described in (Sipe et al. 2016, Lowery et al. 2017). Briefly, V1 and Cb sections were rinsed in RT 0.1M PBS (three 10 minute washes) and incubated in a methanol/hydrogen peroxide block to quench endogenous peroxidases and blocked in bovine serum albumen (BSA). Sections were incubated in primary antibody solution for 48hrs at 4°C on a shaker in a humidified chamber (anti-IBA-1 1:2500, Wako 019–19741). The sections were then washed with 0.1M PBS and left for 4 hours at RT in secondary antibody (Alexa-Fluor 594 1:500, donkey anti-rabbit; Invitrogen A21207).

For qualitative evaluation of P2RY12 expression, sections were incubated with primary antibody (rabbit-anti-P2RY12 1:2000, Anaspec AS-55043A) overnight at 4ºC (in PBS containing 0.3% Triton-X and 0.5% BSA). Sections were washed in PBS and incubated with

secondary antibody (Alexa-Fluor 594 1:500, goat anti-rabbit; Invitrogen A11012). Sections were mounted onto glass slides with coverslips using Prolong Gold (Molecular Probes, P36934).

## Quantitative Analysis of Microglial Morphology and Density in Fixed Tissue

In all experiments, layers in V1 and Cb were identified using DAPI labeling. 5 CX3CR1-GFP adult mice, and 3 Ai9/L7Cre/CX3CR1-GFP adult mice were used for morphology and density experiments, with only the GFP expression intrinsic to the microglia used to locate and characterize the morphology of these cells. The Iba-1 and CX3CR1-GFP co-labeling experiment had n=3 V1 and n=4 Cb with 2–4 sections analyzed per animal. Results were similar across genotypes and were therefore pooled in the analysis presented. Only microglia with all processes visible within the imaged area were included for either density or morphology analysis.

**Microglia arbor complexity—**Coronal sections containing layer 1/2 of V1 or the molecular layer (ML) of the Cb were imaged using a Zeiss LSM 510 confocal microscope (Carl Zeiss). A 40× magnification objective (1.2 NA water-immersion objective) was used, and z-stacks were collected using a 1μm step size. Prior to Sholl Analysis, which was used to determine the branching complexity of the microglial arbor, 20 Z planes were projected into a maximum intensity image. A subset of microglia per image (numbered and randomly selected using a random number generator) were then carefully selected from the original image, thresholded, and binarized. Utilizing the Sholl Analysis plugin in ImageJ (developed by the Anirvan Ghosh laboratory), concentric circles were drawn over each selected microglia radiating out from the soma at 2μm intervals until the entire process arbor was encompassed. The number of intersections between the microglial arbor and each concentric circle were quantified. Results per animal in each brain region were an average of Sholl data from 15 microglia.

**Microglial cell markers—**Coronal sections of V1 and Cb were imaged using a Zeiss LSM 510 confocal microscope. A 20× magnification objective (1.2 NA water-immersion objective) was used, and z-stacks were collected using a 1μm step size. Iba-1and CX3CR1-GFP co-labeling was calculated from 20× images utilizing the following formula: (# Iba-$1^{POS}$and $GFP^{POS}$ microglia) / (# Iba-$1^{POS}$ microglia). For P2RY12 qualitative co-labeling, images were also collected at 40x.

**Microglial density—**Epifluorescent images were collected (microglia in green and nuclei in blue) utilizing an Olympus Bx51 microscope (Olympus, 10x/0.30) and captured with Spot Pursuit digital camera and Spot Advanced software (Sony). Layer 1–3 and 4–6 of V1 as well and the Molecular Layer (ML)/Purkinje neuron layer (PCL) and granular layer (GL) in Cb were outlined in ImageJ using the polygon tool, and the area was measured. The paintbrush tool was used to mark each microglial cell body. Results from 3 sections per animal were averaged. Density per region was calculated at the number of microglia/area in $mm^3$, where the thickness of the section was 50μm.

### Cranial window surgery

Animals were anesthetized using isoflurane (ISO flow rate ~1–2%) during the cranial window implantation surgical procedure. Lubricant ointment was used to keep the eyes moist and protected. Body temperature was maintained at 37°C during the surgery. Aseptic technique was adhered to during all surgical procedures: all tools were autoclaved for steam sterilization, and tools were sterilized in a bead sterilizer between surgeries (up to 3 times). Mice were mounted in a stereotaxic frame and head-fixed for surgical procedures. The skull was exposed through a scalp incision and all connective tissues were cleared off the skull. A 3mm biopsy punch (Integra) was then used to create a circular score on the skull over either V1 or the Cb. A 0.5 mm drill bit (FST) was used to then drill through the skull for the craniotomy, tracing the 3mm score. A 5mm coverslip attached to a 3mm coverslip (Warner Instruments) by UV glue (Norland Optical Adhesive, Norland Inc) was then slowly lowered down into the craniotomy (3mm side down). The coverslip was carefully secured with Loctite 404 glue (Henkel Corp). A custom headplate produced by emachine shop (www.emachineshop.com) (designs courtesy of the Mriganka Sur Lab, MIT) was then secured onto the skull utilizing C&B metabond dental cement (Parkell Inc). The cement was then used to cover the rest of skull and seal the incision site. Animals were administered Buprenorphine (5 mg/kg) analgesic every 12hrs for 3 days and given a minimum of 2 weeks to recover from surgery prior to imaging sessions.

### Two-photon microscopy

A custom two-photon laser-scanning microscope was used for *in vivo* imaging (Ti:Sapphire, Mai-Tai, Spectra Physics; modified Fluoview confocal scan head, 20× water-immersion objective, 0.95 numerical aperture, Olympus). Excitation for fluorescent imaging was achieved with 100-fs laser pulses (80MHz) at 920nm with a power of ~40mW measured at the sample. For motility experiments in CX3CR1-GFP mice a 580/180 (GFP) filter was used. For experiments in Ai9/L7Cre+/CX3CR1-GFP mice a 565 dichroic with 520/40 (GFP) and 578/105 (tdTomato) filters were used. During all imaging sessions mice were anesthetized with a fentanyl cocktail consisting of fentanyl (0.05 mg/kg, i.p.), midazolam (5.0 mg/kg, i.p.), and dexmetatomadin (0.5 $mgkg^{-1}$). During imaging sessions and during post imaging recovery, mice were kept at 37°C until they were alert. Imaging was conducted at 1–4 digital zoom and 1μm z-step, with time-lapse imaging at 5 minute intervals over 1 hour. Image analysis was done offline using ImageJ and Matlab with custom algorithms as described in Sipe et al. 2016 and available upon request. In our imaging sessions we did note a small degree of bleed-through of the tdTomato fluorescence into the background of our GFP channel. This was likely due to the filters selected, and was only apparent once the images were being processed in ImageJ. This did not interfere with selection and isolation of microglia for any of our measures.

**Microglial motility and surveillance—**Microglial motility analysis was performed in ImageJ and Matlab as previously described (Sipe et al., 2016). Z-stacks were collected in V1 or the Cb every 5 minutes for 1 hour, producing 12 time points. All z-stacks were between 55–60μm and for analysis, uniform z-projections were made (20μm thick). For cerebellar imaging, images of Purkinje neurons in the red channel were used to select sections of the stack that were either in the ML or PCL, and lateral motion artifact was corrected (Stackreg

plugin, ImageJ). A threshold was applied to all images, and color overlays were generated for adjacent sets of time points, resulting in 11 overlay images where red pixels represent processes present in only the first time point (retraction), green pixels represent processes present in only the second time point (extension), and yellow pixels represent processes present in both adjacent time points (stability). A custom Matlab algorithm (Sipe et al., 2016) was used to compare pixels across individual time points or across consecutive time point overlays to generate a motility index (defined as the sum of all red and green pixels divided by all yellow pixels). For each index, all microglia in the Z-projection of the imaging session were analyzed to generate the value per animal for the 1-hour session. The thresholded time points were also used to calculate the area monitored (surveillance measurement) by microglia during the 1-hour imaging session. This was done by collapsing the 12 time points through the z-projection function in ImageJ and calculating the total number of pixels representing microglia normalized to the number of pixels in the first time point.

**Soma motility—**For analysis of individual microglial motility in stable and motile somas, single microglial cells were selected in ImageJ and subjected to the same motility analysis program utilized for total microglial motility. To generate stable versus motile soma motility measurements per animal, 2 motile and 2 stable cells were selected from each of the imaging sessions and their motility indices were averaged. In order to evaluate how soma motility impacted microglial distribution over time, animals were imaged at 0 and 7 days. The same region of Cb or V1 was located 7 days after the first imaging session by utilizing vasculature patterns. Stacks of 100μm taken on day 0 and day 7 were aligned in the z direction based on the vasculature. To obtain a quantification of soma movement over 7 days, a nearest neighbor analysis was performed: the coordinates (x,y,z) of each microglial soma was recorded on day 0, and then the nearest soma to those coordinates was found on day 7. This was done for all somas visible in the 100μm stack. The vector of the distance between the day 0 and day 7 coordinates was found for all the somas to generate average nearest neighbor values for all the animals. For V1 and Cb, the same animals were used as the windows implanted spanned both regions.

**Laser ablation—**Laser ablation injuries were created by running a point scan for 8s at 780nm using ~75mW at the sample. The microglial injury response was measured as previously described (Gyoneva et al., 2014; Nimmerjahn et al., 2005). Z-stacks of 40–50μm were collected every 5 minutes. For analysis, z-projections were all comprised of 10μm of the stack, above and below the estimated center of the ablation core. The area of the laser ablation core was traced and measured at time 0. At each of the 12 time points the border of the most proximal tips of the microglial processes was traced and the enclosed area measured to gauge how rapidly the processes reached the core (Fig. 6). The area of the core at each timepoint was subtracted from the area measurements at each time point to normalize the measurements.

**Microglial interactions with Purkinje neurons—**Microglial interactions with Purkinje cells were recorded in 1 hour imaging sessions. Stacks of 60 μm were collected which spanned both ML and PCL layers. Contacts between microglia and dendrites and dendritic

BPs were identified at all time points and their duration was quantified. In order to better validate the presence of these putative microglial Purkinje neuron contacts, 3-D reconstructions of the stacks were rendered utilizing Imaris software (Bitplane, South Windsor, CT).

### Statistics

Statistical tests were run utilizing Prism V5 statistical analysis software (GraphPad) and are described in the text for each experiment. The n's for the experiments represent individual animals. Reported values are the mean ± s.e.m. For all analyses, $\alpha$=0.05.

## RESULTS

To characterize the behavior of cerebellar microglia during physiological brain function, we utilized the CX3CR1-GFP mouse in which microglia throughout the brain express Green Fluorescent Protein (GFP) under control of the CX3CR1 promoter (Jung et al., 2000). This allowed us to visualize microglia in the Cb and cortex of the adult mouse *in vivo* and *in situ*. In some cases CX3CR1-GFP mice were bred to Ai9/L7cre mice in which tdTomato is expressed in Purkinje neurons, allowing us to visualize the interactions between cerebellar microglia and these neurons.

### Microglial density and morphology in the Cb

We first sought to determine whether microglia in the Cb were similarly distributed as compared to other populations that have been extensively studied. Therefore we compared the density of GFP-labeled microglia in fixed sections of the adult Cb to microglial density in V1 of the same animals. Qualitatively, microglial density was lower in the Cb, with microglia not tiling the Cb as completely as they do the cortex (See supplemental videos 1 (V1) and 2 (Cb)). We observed a significant difference in microglial density in both the granular (GL) and Molecular layer (ML)/Purkinje cell layer (PCL) layers of the Cb when compared to V1 layers 1–3 and layers 4–6 (Figure 1, n=8 One-Way repeated measures ANOVA $p<0.0001$, Bonferroni *post hoc* test, GL v. V1 1–3 & V1 4–6 $p<0.0001$, ML/PCL v. V1 1–3 & V1 4–6 $p<0.0001$). The density of microglia in the GL was also higher than that of microglia in the ML/PCL (GL and ML/PCL *post hoc* comparison, $p<0.05$).

Because we were using the GFP signal as a label for microglia we wanted to confirm that the difference in density was not due to incomplete labeling of microglia based on GFP expression driven by the CX3CR1 promoter. Using immunohistochemistry for Iba-1, a reliable microglial marker, we confirmed that 91.48%±0.43% of Iba-1 labeled microglia also expressed GFP in the Cb and 98.98% ± 0.53% expressed GFP in V1 (Figure 1C, D, & F). While co-labeling in the Cb was lower than in V1 it could not account for the marked difference in microglial density between the two regions.

In addition to this large disparity in microglial density between the Cb and V1, we observed significant differences in microglial arbor ramification. Morphologically, cerebellar microglia appear less ramified than microglia in V1, with fewer secondary and tertiary processes (Figure 2). To quantify our observations we used Sholl analysis on confocal images of microglia obtained in the two brain areas. While both cerebellar (ML) and cortical

(layer ½) microglia had a similar number of primary processes (~3) and similar arbor spread (radius ~50μm), cerebellar microglia were significantly less ramified starting between 2 μm and 38 μm from the soma (Two-way repeated measures ANOVA, $p<0.0001$, Bonferroni *post hoc* tests, from 2–36μm $p<0.0001$ and at 38um $p<0.001$). The maximum number of intersections in cortical microglia reached ~9 at a distance of ~15μm from the soma, whereas cerebellar microglia showed a maximum number of intersections of only ~4 at a similar distance, suggesting that arborization is less complex in these microglia. The significance of microglial morphology in the absence of pathological events is not clear, but it is known that microglia change their structure based on their immunological state (Hanisch and Kettenmann, 2007). Thus these findings may suggest that cerebellar microglia are functionally unique from cortical microglia. Previous reports have suggested the expression of P2RY12 is related to microglial ramification and activation state (Eyo et al., 2014; Haynes et al., 2006; Ohsawa et al., 2007; Sipe et al., 2016). To determine whether microglial morphology in Cb was driven by differences in P2RY12 expression, we used immunohistochemistry and found that the less ramified microglial arbors in Cb expressed high levels of P2RY12 in their processes (Figure 2 D, E). These results suggest that microglia in Cb may not be immunologically primed but have a distinct basal function.

## The dynamic behavior of cerebellar microglia

While a handful of previous studies characterized the static morphological characteristics of cerebellar microglia, these cells are highly motile *in vivo*, allowing them to rapidly survey the parenchyma and perform homeostatic functions in the brain. Therefore, after assessing the distribution and morphology of cerebellar microglia, we wanted to determine if the differences in morphology were reflected in their dynamic function and whether the decreased density and altered arbor complexity had an impact on the rate at which cerebellar microglia interact with the CNS milieu. Despite the differences in morphology, when cerebellar microglia in the superficial layers (0–75um below the level of the pia) were compared to cortical microglia, we found that there were no significant difference in their motility as assayed using a motility index (see methods; Figure 3A–C, n=4 V1, n=7 ML, t-test. See supplemental videos 3 V1 and 4 Cb). Therefore, although microglia of the Cb are significantly less ramified, they are still moving their processes at a similar rate to their more ramified V1 counterparts. However, we did find that within the same animal, microglia within different layers of the Cb exhibited different motility. Microglia within the PCL exhibited a higher rate of motility when compared to more superficial microglia within the ML, where the dendritic arbors of the Purkinje neurons reside (Figure 3D, n=5, paired student's t-test, $p<0.05$), suggesting that microglia may have layer-specific roles in the cerebellar cortex.

While it was surprising to us that cerebellar microglia exhibited similar levels of motility to cortical microglia, despite the difference in their morphology, we suspected that cerebellar microglia surveyed less of the brain parenchyma than cortical microglia in a similar time frame. To assay microglial surveillance, we superimposed images taken at all 12 time points of the hour imaging session, quantified the area occupied by microglial processes, and defined this as a "% surveillance. We found that cerebellar microglia in both the ML and PCL survey less territory in the course of a 1 hour imaging session when compared to V1

microglia (% coverage; Figure 4 n=4 V1, n= 7 ML, n=5 PCL, One-way ANOVA, Bonferroni *post hoc* tests, $p<0.01$ for V1 v. ML and V1 v. PCL). To determine whether this was a function of the reduced arborization of cerebellar microglia, we normalized the surveillance over the whole imaging session to that at the first time point. Interestingly, we found that deep cerebellar microglia in the PCL surveyed the CNS at a higher rate than the V1 microglia (surveillance ratio; Figure 4, n=4 V1, n= 7 ML, n=5 PCL, One-way ANOVA, Bonferroni *post hoc* tests, $p<0.01$ for V1 v. PCL). Although in total these deeper cerebellar microglia are not able to cover as much territory in an hour, they are surveying more parenchyma with respect to their density and process arbor than the V1 microglia. ML microglia showed an intermediate phenotype that was not significantly different from V1 or PCL microglia.

Additionally, cerebellar microglia in both the ML and PCL exhibited motile somas, a phenomenon that has not been routinely described in other parts of the brain (Davalos et al., 2005; Nimmerjahn et al., 2005; Sipe et al., 2016; Tremblay et al., 2010; Wake et al., 2009). In multiple instances across different animals, we observed a change in the structure and a shifting of the position of cell soma in conjunction with process movement and on a similar timescale (minutes; Figure 5; See supplemental video 5). This was not an artifact of cranial window implantation, as we never saw somal movement in V1 using cranial windows. We also made this observation in animals with windows that spanned both the Cb and V1. In total there were 36 instances of soma motility across all the cerebellar imaging sessions, and 0 instances in all V1 imaging sessions. We observed a total of 173 cerebellar microglia and 83 V1 microglia (n=6 V1, and n=13 Cb mice, totals refer to all microglia in all animals studied). On average, 20.8% of cerebellar microglia exhibited soma motility (ranging from 0%−41% of microglia per animal). Interestingly, the largest soma translocations were preceded by a large retraction (38.8% of motile somas) or extension (13.9% of motile somas) of a primary process. The remaining soma movements observed could be classified as small shifts of soma cytoplasm in within the x,y, or z planes.

We analyzed the motility indices of individual microglia with either stable or motile somas in order to evaluate if soma motility increased the overall motility of microglia. We found that within the same mice, microglia with motile somas had a greater motility index, showing that there is a positive correlation between somal motility and overall motility (Figure 5C, n=5, paired student's t-test, $p<0.05$). We next asked if these increased soma movements would result in changes in microglial distribution over longer periods of time. To answer this, we imaged the same regions in V1 and Cb at 0 and 7 days. Utilizing nearest neighbor analysis we found that on average V1 microglia were within 5 μm of their original locations and Cb microglia were found an average of 25μm from their day 0 location after 7 days (Figure 5D–F, n=4 V1, n=9 Cb, Student's t-test $t(11)=5.898$, $p<0.0001$). This analysis underestimates the migration of microglia over time as it does not identify the movement of each microglia, but rather identifies the nearest location to which a single soma might have migrated, suggesting that microglial redistribution across the Cb could be extensive over time.

To determine whether cerebellar microglia responded similarly to V1 microglia in the context of a pathological stimulus, we induced a focal brain injury using the two-photon

laser and subsequently quantified the movement of microglial processes toward the site of injury over 1 hour. Both cerebellar and V1 microglia responded rapidly to acute focal brain injury. In fact, Cb microglia reached the core at 30 minutes, the same time-point as the V1 microglia despite traversing a significantly larger amount of parenchyma. Quantitatively, we found that from 0–20 minutes post-injury, Cb microglial processes were significantly further away from the lesion core before reaching the core at the same time as the V1 processes (Figure 6, n=6 V1 and n=5 Cb, Two-way repeated measures ANOVA; See Supplemental videos 6 V1 and 7 Cb). Despite similar basal rates of motility, Cb microglia react more robustly and are able to reach injury sites across greater distances at the same rate as V1 microglia.

## Interactions between cerebellar microglia and Purkinje neurons

Because microglia have been reported to interact with neuronal elements in the cortex, we wanted to characterize these interactions in the Cb. We therefore labeled Purkinje neurons using the transgenic line Ai9/L7-cre where all Purkinje neurons express tdTomato and bred it to our CX3CR1-GFP line (Figure 7– 8). As has been reported for microglia and dendrites in the cortex, we observed dynamic and intimate interactions between cerebellar microglia and Purkinje neuron dendrites varying in duration from transient 5 minute to lengthy 60 minute interactions (Figure 7 C–D). These interactions took different forms: 1. We observed many instances of microglial processes making contacts along the length of the Purkinje neuron dendrites; rapidly retracting and extending along the dendrite within as little as 20–30 minutes (Figure 7A–D; marked with arrowheads; See supplemental videos 8, 9, and 12); 2. We also observed processes wrapping around dendrites. This was most apparent in dendrites that extended in the Z-direction where it was possible to see the cross-section of the dendrite. The microglia in these instances seem to wrap around the branch points of these dendrites, where a thickening could be seen in the tdTomato signal in the z-projected images and in the 3D-reconstructions (Figure 7A–D; marked with an arrow); 3. Other microglia extended processes across the axis of the dendrites and touched many dendrites in succession (Figure 7A; see yellow arrowheads). These diverse process extensions and interactions suggest that a given cerebellar microglia is capable of simultaneously sampling many dendrites rapidly, possibly permitting detection of changes in neural network activity. The average duration of microglial contacts was on the order of 40 minutes and was similar in the first two modes of contact described above (Figure 7D).

At the level of the PCL, microglial processes extended and retracted, making putative contacts with the somas of Purkinje neurons (Figure 8; See supplemental videos 10, 11, and 13). Microglial cell somas were interspersed between the Purkinje neuron somas and could be observed moving around the cells effectively forming a C-shape wrapped around the neuronal soma (Figure 8 D, microglia 1; See supplemental video 13). Additionally, microglial processes often wrapped around, and remained in close proximity to, Purkinje cell somas as they retracted and extended (Fig. 8B–C). Most microglial arbors were in contact with 4–8 Purkinje neuron somas at any one time and no clear patterns of retraction or extension were noted based on the interaction with any particular cell body. The processes in contact with somas at times seems to create a webbing over the soma, effectively sampling an entire side of the cell body. Microglial soma sampling by bulbous process

endings has also been previously observed in the zebrafish, suggesting that this might be an important aspect of microglia surveillance of neurons (Li et al., 2012). These Purkinje layer microglia had the highest rate of surveillance, which may indicate that sampling of Purkinje neuron somas is of particular functional importance in the Cb (Figure 5D). Such robust interactions and monitoring of multiple somas simultaneously could allow microglia to respond to changes in neural activity associated with plasticity or damage. Future work could confirm these contacts at the ultra-structural level and also determine how these contacts may change under different conditions such as disease and injury.

## DISCUSSION

Here we have characterized the *in vivo* behavior of physiological cerebellar microglia for the first time and compared this behavior to that observed in cortical microglia, which have been better studied. We found that cerebellar microglia are less densely distributed than their cortical counterparts in the ML, PCL, and GL. We also demonstrated that the arbor of Cb microglia is far less complex and that they appear almost bipolar with two main processes extending from the soma. Utilizing chronic cranial window implants over the Cb, we were able to observe unperturbed Cb microglia and evaluate their motility and surveillance. We observed that Cb microglia display process motility that is akin to that seen in cortical microglia, despite differences in morphology, but that the somas of Cb microglia are motile and frequently show rapid displacements unlike what is seen in cortex where microglial somas are stable even during chronic imaging sessions that span weeks to months. We found that these somal displacements enhanced individual cell motility and produced changes in microglial distributions over the course of a week. We also demonstrated that microglial processes interact dynamically with both the dendrites and somas of Purkinje neurons in the Cb, similarly to their cortical counterparts (Tremblay et al., 2010; Wake et al., 2009). These interactions were highly variable in duration, which agrees with previous findings in cortex from our lab (Lowery et al., 2017; Tremblay et al., 2010). Our findings suggest that cerebellar microglia may have unique morphological and dynamic behaviors that support different roles that these microglia play in cerebellar function as compared to microglia in other parts of the brain.

### Microglial structure and dynamics

Despite our current understanding of microglia as a cell type that is critical both for normal brain function and for resolving pathological events, few studies have examined cerebellar microglia in detail. Most of the newer studies on cerebellar microglia have focused on development and pathology (Ashwell, 1990; Cardoso et al., 2015; Drew et al., 2015; Grabert et al. 2016; Kane et al., 2011; Marin-Teva et al., 2004; Tay et al. 2017), while older studies, which examined microglial morphology did not examine the dynamic aspect of microglial function (Lawson et al., 1990; Mannoji et al., 1986; Vela et al., 1995). We believe that this study is the first to pair fixed tissue analysis with *in vivo* imaging of cerebellar microglia and provide insight into the dynamic behavior of these cells within their native milieu. In order to image microglia in vivo we used a mouse lacking one copy of CX3CR1, an important receptor for many microglial functions (Arnoux et al., 2013; Lowery et al., 2017; Paolicelli et al., 2014; Schecter et al., 2017). While this has to be taken into account, many of our

results previous studies carried out in wild type animals. Our finding that microglia are distributed at a lower density in the Cb than in cortex confirms previous studies (Lawson et al., 1990; Vela et al., 1995). Like these previous studies we observed significantly higher microglial densities in the GL/PCL than in the ML although the magnitude of this increase was not as great as reported previously. Studies have also suggested that microglial cell bodies are not present in the PCL and that microglia in the ML do not extend their processes towards Purkinje neuron somas (Vela et al. 1995). Our simultaneous *in vivo* imaging of Purkinje neurons and microglia, however, shows a clear co-existence of Purkinje and microglial cell bodies within the PCL and a dynamic and intricate interaction between microglial processes and neuronal somas. In fact, our data suggest that microglia located in the PCL are more dynamic than those in the ML, suggesting that Cb microglia may have distinct behaviors depending on whether they are interacting with Purkinje neuron somas or dendrites. We also quantitatively observed that cerebellar microglia were less ramified than their cortical counterparts, as had been reported qualitatively (Lawson et al., 1990; Vela et al., 1995). These (Hoshiko et al., 2012; Maggi et al., 2011) less ramified microglia are just as motile as highly ramified microglia in the cortex and extend and retract their processes at similar rates. The absolute area explored by microglial processes in a 1 hour period is significantly smaller in the Cb than cortex due to the smaller cerebellar arbor and the lower density of cerebellar microglia. Thus, cerebellar microglia may be less able to survey the parenchyma than microglia in the cortex. It is possible that this reduced surveying ability is compensated in part by somatic motility, whereby microglia in the Cb may translocate continually to different areas of the Cb, unlike cortical microglia, which maintain stable territories.

### Unique roles for cerebellar microglia

Our analysis shows that adult cerebellar microglia have distinct morphological and dynamic attributes compared to cortical microglia, suggesting that these cells may play different roles in adult cerebellar function. The simplification of the process arbor and the motility of the soma suggests that cerebellar microglia may exist in a different functional state than cortical microglia, possibly one that is more akin to immunological activation. Recent analysis of post-mortem human tissue and isolated murine microglia provides credence to this notion (Grabert et al., 2016; Mildner et al., 2017). Cerebellar microglia have higher rates of basal turnover, have increased expression of proinflammatory genes, and are more responsive to perturbations from disease (Grabert et al., 2016; Mildner et al., 2017; Tay et al., 2017), suggesting that they indeed may have a different molecular and functional profile than microglia elsewhere in the brain. Cerebellar microglia also have higher expression of molecules associated with adhesion, cell migration, and metabolism (Grabert et al., 2016). These differences in gene expression may be critically important to enabling cerebellar microglial cell body motility.

During development, cerebellar microglia are integral in pro-apoptotic and proinflammatory processes, which clear away Purkinje neurons to promote normal circuit development (Ashwell, 1990; Marin-Teva et al., 2004). At this stage of development, cerebellar microglia are immature and maintain amoeboid morphologies. It is currently unknown whether cerebellar microglia contribute to the developmental pruning of synapses as circuits develop,

much like microglial roles elsewhere in the brain (Hoshiko et al., 2012; Pagani et al., 2015; Paolicelli et al., 2011; Schafer et al., 2012; Sipe et al., 2016; Stevens et al., 2007; Zhan et al., 2014). Our data suggest that microglial processes in the Cb form dynamic contacts with both dendrites and somas of Purkinje neurons, suggesting that in the Cb microglia could contribute to synaptic rearrangement. The higher motility of processes in the PCL could reflect a higher surveillance of synapses made onto the somas of these cells. The lower density of microglia in both the ML and PCL would make it harder for microglia to interact with a large number of synapses, possibly limiting their roles in plasticity or increasing the delay between activity-driven synaptic changes and microglial recruitment. While the duration of contacts between microglia and neurons is highly variable in the Cb and similar to what has been reported in cortex, it is difficult to directly compare such contacts quantitatively in brain areas where the neuronal architecture is different (Lowery et al., 2017; Tremblay et al., 2010; Wake et al., 2009). However, close apposition of microglial processes and neuronal dendrites over distance (e.g extending along a dendrite) is rarely seen in the cortex, suggesting that the mode of contact may be fundamentally different in the two brain areas. Given our findings, the differences in Cb microglial structure and motility implies that there are basic differences in their physiological function in the Cb compared to their cortical counterparts.

The close interaction and surveillance of Purkinje neurons by microglial processes is likely critically important to disease processes as well. Previous work has shown that postnatal ethanol exposure, which leads to altered Cb function in the adult, activates Cb microglia and readily drives IL-1β and TNF-α production (Drew et al., 2015; Kane et al., 2011). Such changes in microglial activation state are accompanied by Purkinje neuron death and altered circuit development. With microglia so intimately interspersed amongst the Purkinje neurons, any perturbation such as alcohol exposure may rapidly produce microglial driven neuronal changes or damage (Grabert et al., 2016; Tay et al., 2017). While our work did not begin to address toxins or disease in the Cb, our imaging paradigm and new findings on cerebellar microglia open the door to future study of disease states and microglial responses to disorders of the Cb. We observed a more rapid response in cerebellar microglia to focal tissue injury which suggests that cerebellar microglia may have a more immunologically activated resting state as is evidenced by their higher expression of immunological markers (Grabert et al., 2016). This sort of acute localized injury, however, does not wholly recapitulate how microglia may respond to more widespread or nuanced disease and injury. We hope that with a better understanding of the unique nature and distribution of cerebellar microglia, we will be better able to study perturbations of these cells. Our finding that motility differs at different depths within the Cb also suggests that something similar could be found in other brain regions and hopefully future studies will attempt to target potential *in vivo* heterogeneity of microglial physiology. With a better understanding of the unique geographical profiles of microglia throughout the CNS we may be able to elucidate the basis for regional vulnerabilities to CNS disease and disorders.

## CONCLUSIONS

Here we have shown that cerebellar microglia are a specialized population of cells with decreased ramification and cell density compared to cortical microglia. They are closely

associated with Purkinje neurons and make putative contacts during process motility with both their somas and dendrites. With these findings, future work will be able to target how microglia may participate in cerebellar plasticity and how they may also interact with other cerebellar neuronal cell types. Additionally the physiology of cerebellar microglia likely impacts disease progression and a better understanding of their baseline characteristics will lead to a better understanding of diseases rooted in cerebellar dysfunction.

## Supplementary Material

Refer to Web version on PubMed Central for supplementary material.

## REFERENCES

Arnoux I, Hoshiko M, Mandavy L, Avignone E, Yamamoto N, Audinat E, 2013 Adaptive phenotype of microglial cells during the normal postnatal development of the somatosensory “Barrel” cortex. Glia 61, 1582–1594. [PubMed: 23893820]

Ashwell K, 1990 Microglia and cell death in the developing mouse cerebellum. Brain research. Developmental brain research 55, 219–230. [PubMed: 2253324]

Cardoso FL, Herz J, Fernandes A, Rocha J, Sepodes B, Brito MA, McGavern DB, Brites D, 2015 Systemic inflammation in early neonatal mice induces transient and lasting neurodegenerative effects. Journal of neuroinflammation 12, 82. [PubMed: 25924675]

Davalos D, Grutzendler J, Yang G, Kim JV, Zuo Y, Jung S, Littman DR, Dustin ML, Gan WB, 2005 ATP mediates rapid microglial response to local brain injury in vivo. Nat Neurosci 8, 752–758. [PubMed: 15895084]

Drew PD, Johnson JW, Douglas JC, Phelan KD, Kane CJ, 2015 Pioglitazone blocks ethanol induction of microglial activation and immune responses in the hippocampus, cerebellum, and cerebral cortex in a mouse model of fetal alcohol spectrum disorders. Alcohol Clin Exp Res 39, 445–454. [PubMed: 25703036]

Eyo UB, Peng J, Swiatkowski P, Mukherjee A, Bispo A, Wu LJ, 2014 Neuronal hyperactivity recruits microglial processes via neuronal NMDA receptors and microglial P2Y12 receptors after status epilepticus. J Neurosci 34, 10528–10540. [PubMed: 25100587]

Grabert K, Michoel T, Karavolos MH, Clohisey S, Baillie JK, Stevens MP, Freeman TC, Summers KM, McColl BW, 2016 Microglial brain region-dependent diversity and selective regional sensitivities to aging. Nature neuroscience 19, 504–516. [PubMed: 26780511]

Gyoneva S, Davalos D, Biswas D, Swanger SA, Garnier-Amblard E, Loth F, Akassoglou K, Traynelis SF, 2014 Systemic inflammation regulates microglial responses to tissue damage in vivo. Glia 62, 1345–1360. [PubMed: 24807189]

Hanisch UK, Kettenmann H, 2007 Microglia: active sensor and versatile effector cells in the normal and pathologic brain. Nature neuroscience 10, 1387–1394. [PubMed: 17965659]

Haynes SE, Hollopeter G, Yang G, Kurpius D, Dailey ME, Gan WB, Julius D, 2006 The P2Y12 receptor regulates microglial activation by extracellular nucleotides. Nat Neurosci 9, 1512–1519. [PubMed: 17115040]

Hoshiko M, Arnoux I, Avignone E, Yamamoto N, Audinat E, 2012 Deficiency of the microglial receptor CX3CR1 impairs postnatal functional development of thalamocortical synapses in the barrel cortex. J Neurosci 32, 15106–15111. [PubMed: 23100431]

Jung S, Aliberti J, Graemmel P, Sunshine MJ, Kreutzberg GW, Sher A, Littman DR, 2000 Analysis of fractalkine receptor CX(3)CR1 function by targeted deletion and green fluorescent protein reporter gene insertion. Molecular and cellular biology 20, 4106–4114. [PubMed: 10805752]

Kane CJ, Phelan KD, Han L, Smith RR, Xie J, Douglas JC, Drew PD, 2011 Protection of neurons and microglia against ethanol in a mouse model of fetal alcohol spectrum disorders by peroxisome proliferator-activated receptor-gamma agonists. Brain Behav Immun 25 Suppl 1, S137–145. [PubMed: 21376806]

Lawson LJ, Perry VH, Dri P, Gordon S, 1990 Heterogeneity in the distribution and morphology of microglia in the normal adult mouse brain. Neuroscience 39, 151–170. [PubMed: 2089275]

Li Y, Du XF, Liu CS, Wen ZL, Du JL, 2012 Reciprocal regulation between resting microglial dynamics and neuronal activity in vivo. Dev Cell 23, 1189–1202. [PubMed: 23201120]

Lowery RL, Tremblay ME, Hopkins BE, Majewska AK, 2017 The microglial fractalkine receptor is not required for activity-dependent plasticity in the mouse visual system. Glia 65, 1744–1761. [PubMed: 28836393]

Maggi L, Scianni M, Branchi I, D'Andrea I, Lauro C, Limatola C, 2011 CX(3)CR1 deficiency alters hippocampal-dependent plasticity phenomena blunting the effects of enriched environment. Front Cell Neurosci 5, 22. [PubMed: 22025910]

Mannoji H, Yeger H, Becker LE, 1986 A specific histochemical marker (lectin Ricinus communis agglutinin-1) for normal human microglia, and application to routine histopathology. Acta Neuropathol 71, 341–343. [PubMed: 3541481]

Marin-Teva JL, Dusart I, Colin C, Gervais A, van Rooijen N, Mallat M, 2004 Microglia promote the death of developing Purkinje cells. Neuron 41, 535–547. [PubMed: 14980203]

Mildner A, Huang H, Radke J, Stenzel W, Priller J, 2017 P2Y12 receptor is expressed on human microglia under physiological conditions throughout development and is sensitive to neuroinflammatory diseases. Glia 65, 375–387. [PubMed: 27862351]

Miyamoto A, Wake H, Ishikawa AW, Eto K, Shibata K, Murakoshi H, Koizumi S, Moorhouse AJ, Yoshimura Y, Nabekura J, 2016 Microglia contact induces synapse formation in developing somatosensory cortex. Nature communications 7, 12540.

Nimmerjahn A, Kirchhoff F, Helmchen F, 2005 Resting microglial cells are highly dynamic surveillants of brain parenchyma in vivo. Science 308, 1314–1318. [PubMed: 15831717]

Ohsawa K, Irino Y, Nakamura Y, Akazawa C, Inoue K, Kohsaka S, 2007 Involvement of P2X4 and P2Y12 receptors in ATP-induced microglial chemotaxis. Glia 55, 604–616. [PubMed: 17299767]

Pagani F, Paolicelli RC, Murana E, Cortese B, Di Angelantonio S, Zurolo E, Guiducci E, Ferreira TA, Garofalo S, Catalano M, D'Alessandro G, Porzia A, Peruzzi G, Mainiero F, Limatola C, Gross CT, Ragozzino D, 2015 Defective microglial development in the hippocampus of Cx3cr1 deficient mice. Frontiers in cellular neuroscience 9, 111. [PubMed: 25873863]

Paolicelli RC, Bisht K, Tremblay ME, 2014 Fractalkine regulation of microglial physiology and consequences on the brain and behavior. Front Cell Neurosci 8, 129. [PubMed: 24860431]

Paolicelli RC, Bolasco G, Pagani F, Maggi L, Scianni M, Panzanelli P, Giustetto M, Ferreira TA, Guiducci E, Dumas L, Ragozzino D, Gross CT, 2011 Synaptic pruning by microglia is necessary for normal brain development. Science 333, 1456–1458. [PubMed: 21778362]

Parkhurst CN, Yang G, Ninan I, Savas JN, Yates JR 3rd, Lafaille JJ, Hempstead BL, Littman DR, Gan WB, 2013 Microglia promote learning-dependent synapse formation through brain-derived neurotrophic factor. Cell 155, 1596–1609. [PubMed: 24360280]

Schafer DP, Lehrman EK, Kautzman AG, Koyama R, Mardinly AR, Yamasaki R, Ransohoff RM, Greenberg ME, Barres BA, Stevens B, 2012 Microglia sculpt postnatal neural circuits in an activity and complement-dependent manner. Neuron 74, 691–705. [PubMed: 22632727]

Schecter RW, Maher EE, Welsh CA, Stevens B, Erisir A, Bear MF, 2017 Experience-Dependent Synaptic Plasticity in V1 Occurs without Microglial CX3CR1. J Neurosci 37, 10541–10553. [PubMed: 28951447]

Sipe GO, Lowery RL, Tremblay ME, Kelly EA, Lamantia CE, Majewska AK, 2016 Microglial P2Y12 is necessary for synaptic plasticity in mouse visual cortex. Nature communications 7, 10905.

Stevens B, Allen NJ, Vazquez LE, Howell GR, Christopherson KS, Nouri N, Micheva KD, Mehalow AK, Huberman AD, Stafford B, Sher A, Litke AM, Lambris JD, Smith SJ, John SW, Barres BA, 2007 The classical complement cascade mediates CNS synapse elimination. Cell 131, 1164–1178. [PubMed: 18083105]

Tay TL, Mai D, Dautzenberg J, Fernandez-Klett F, Lin G, Sagar, Datta M, Drougard A, Stempfl T, Ardura-Fabregat A, Staszewski O, Margineanu A, Sporbert A, Steinmetz LM, Pospisilik JA, Jung S, Priller J, Grun D, Ronneberger O, Prinz M, 2017 A new fate mapping system reveals context-dependent random or clonal expansion of microglia. Nature neuroscience 20, 793–803. [PubMed: 28414331]

Tremblay ME, Lowery RL, Majewska AK, 2010 Microglial interactions with synapses are modulated by visual experience. PLoS biology 8, e1000527. [PubMed: 21072242]

Vela JM, Dalmau I, Gonzalez B, Castellano B, 1995 Morphology and distribution of microglial cells in the young and adult mouse cerebellum. J Comp Neurol 361, 602–616. [PubMed: 8576417]

Wake H, Moorhouse AJ, Jinno S, Kohsaka S, Nabekura J, 2009 Resting microglia directly monitor the functional state of synapses in vivo and determine the fate of ischemic terminals. J Neurosci 29, 3974–3980. [PubMed: 19339593]

Zhan Y, Paolicelli RC, Sforazzini F, Weinhard L, Bolasco G, Pagani F, Vyssotski AL, Bifone A, Gozzi A, Ragozzino D, Gross CT, 2014 Deficient neuron-microglia signaling results in impaired functional brain connectivity and social behavior. Nature neuroscience 17, 400–406. [PubMed: 24487234]

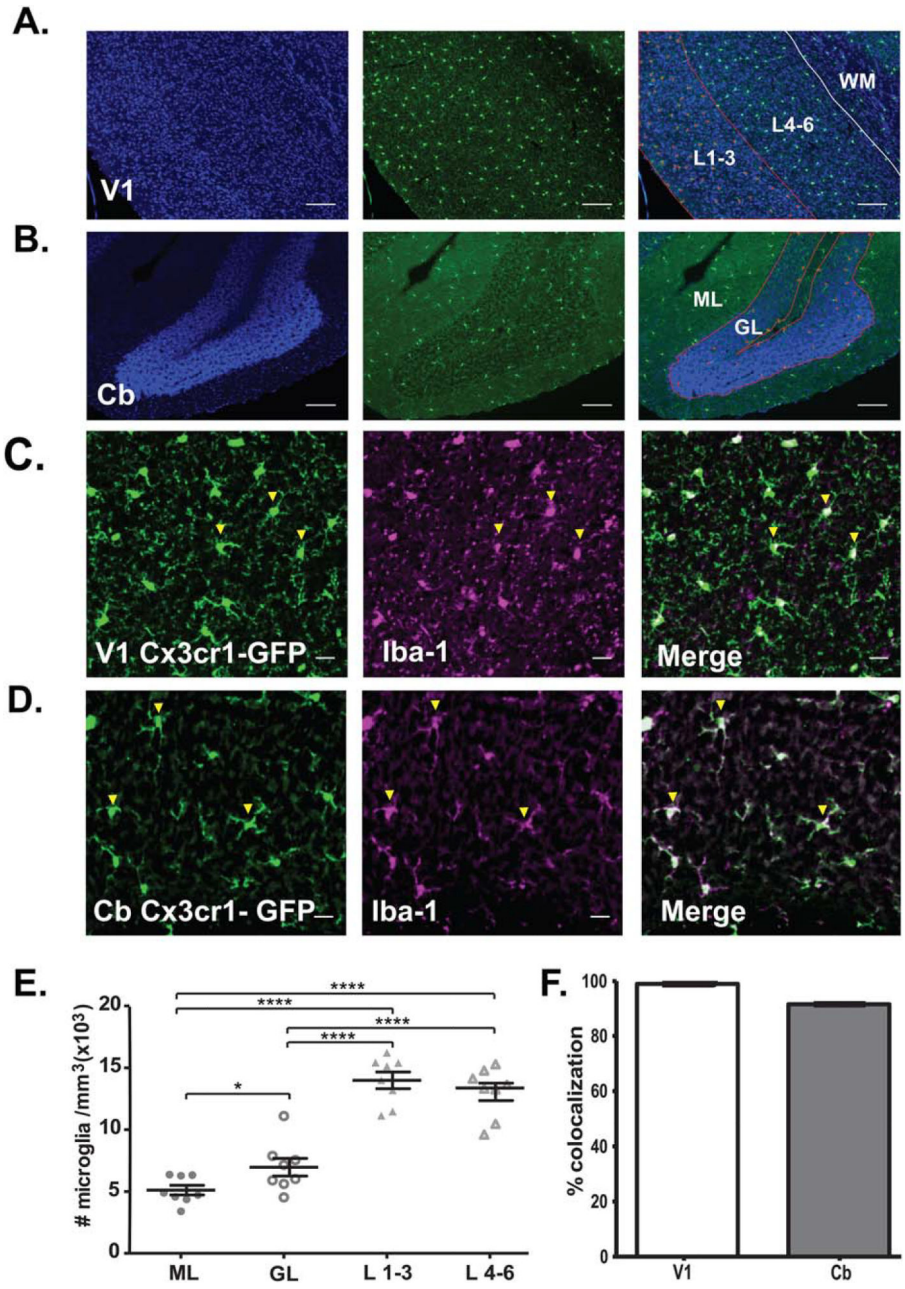


**Figure 1. Microglial are less densely distributed in the cerebellum compared to the visual cortex**

(A-B). Example epifluorescent images of fixed sections of (A.) V1 (B.) Cb in CX3CR1-GFP mice showing cell bodies (DAPI - blue) and microglia (GFP – green). The rightmost panels show merges of the two channels with red lines demarcating examples of regions of interest in V1 and in Cb. Regions of interest included V1 layers 1–3, V1 layer 4–6, the Cb ML/PCL, and the Cb GL. In the V1 example merge image, microglia in layers 4–6 are encompassed by a red outline and marked, as an example of density analysis that was also completed in V1 layers 1–3. The Cb merged image shows an example in which microglial density within the GL was quantified. (C-D). Representative confocal images of microglia in fixed sections of (C.) V1 and (D.) Cb in CX3CR1-GFP mice showing GFP fluorescence (green) and Iba-1

immunoreactivity (magenta). Rightmost panels show merges of the two channels. Representative examples of co-labeled cells designated with yellow arrows. (E.) Microglial density is lowest in the ML/PCL and lower in both the ML/PCL and GL as compared to V1 layers 1–3 and 4–6 (One-way Repeated measures ANOVA $F(3,21)= 118.7$;$P<0.0001$. Bonferroni's Multiple comparisons *post hoc* test for individual comparisons) (F.) Quantification of co-labeling of microglia with Iba-1 and GFP; Scale bars = 100um (A-B.); 20μm (D-E.).

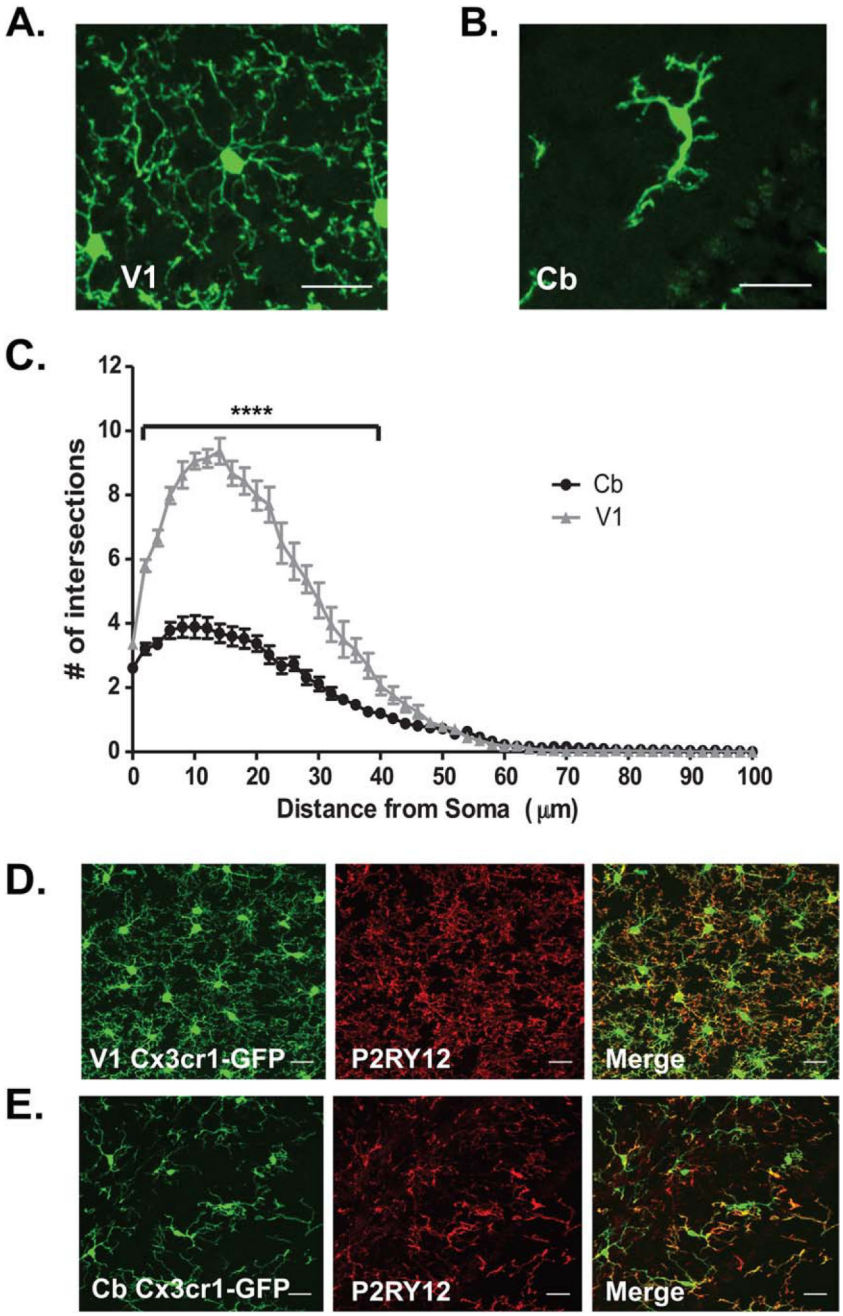


**Figure 2. Cerebellar microglia are less ramified than those in visual cortex**

(A-B). Confocal image of a representative microglia in (A.) V1 and (B.) Cb. Notice that the processes of the V1 microglia are much more ramified than that of the cerebellar microglia. (C.) Sholl analysis demonstrates that cerebellar microglia in the ML have a much less ramified arbor than V1 microglia (Two-way repeated measures ANOVA $F(3,50)=50.21$; $P<0.0001$ from 2μm from soma to 50μm from soma). (D-E). Microglia in V1 (D.) and Cb (E) express P2RY12 in their fine processes. Scale bars=25μm (A & B), and 20μm (D & E).

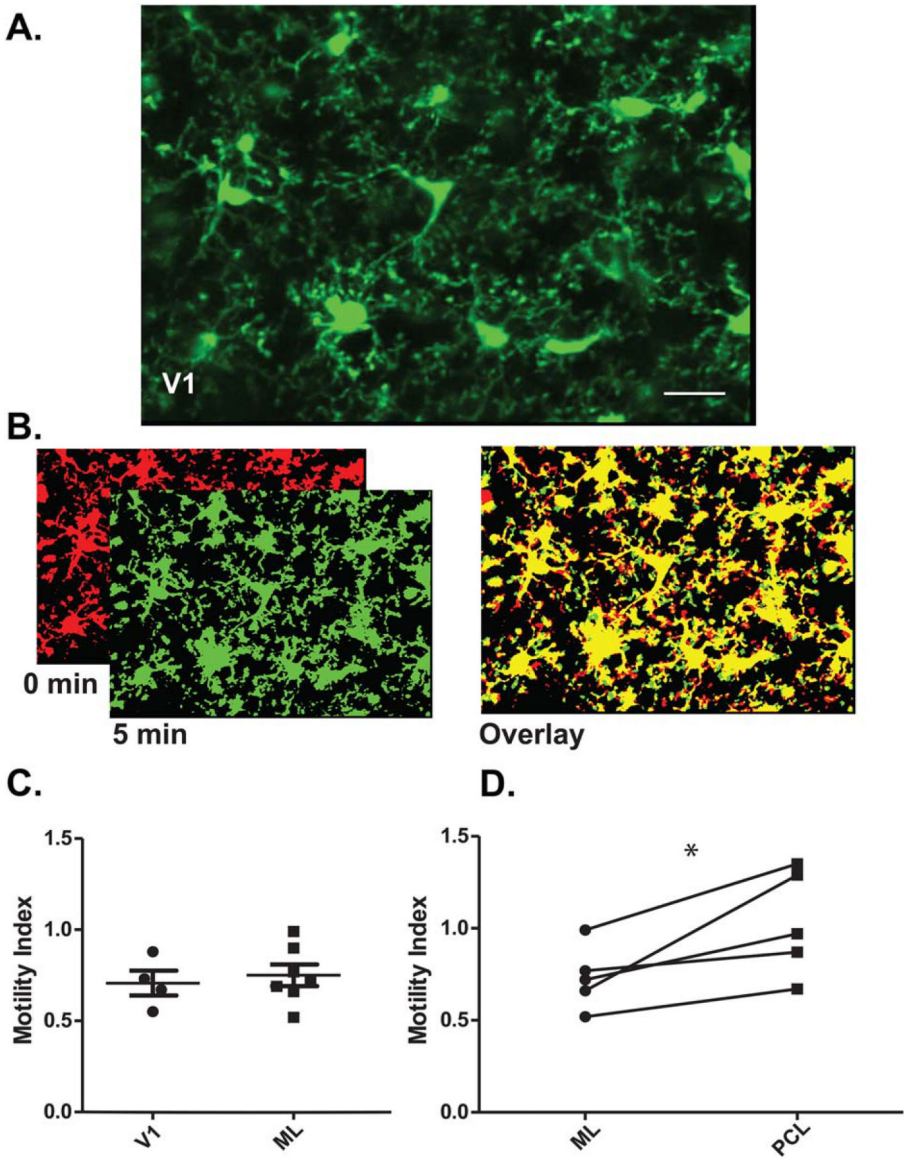


**Figure 3. Cerebellar microglia are as motile as microglia in visual cortex**

(A.) *In vivo* two-photon imaging of V1 microglia through a chronic cranial window. Z-projection of an individual time point. (B.) Examples of thresholded microglia from consecutive time points collected 5 minutes apart where the earlier time point is shown in red and the later time point is shown in green. (C.) RGB overlay of the two thresholded images shown in (B.) used to measure motility. Yellow, green, and red pixels represent stable, extended, and retracted regions respectively. (C.) Cb microglia exhibit similar motility to those in V1 (Student's t-test, $P>0.05$); only superficial microglia (50–150μm from the pia) were included in this analysis. (D.) When compared within the same animal, superficial microglia in the ML are less motile than (D.) microglia in the PCL (paired t-test, $P<0.05$, $t(4)=3.163$). Scale bars =20μm.

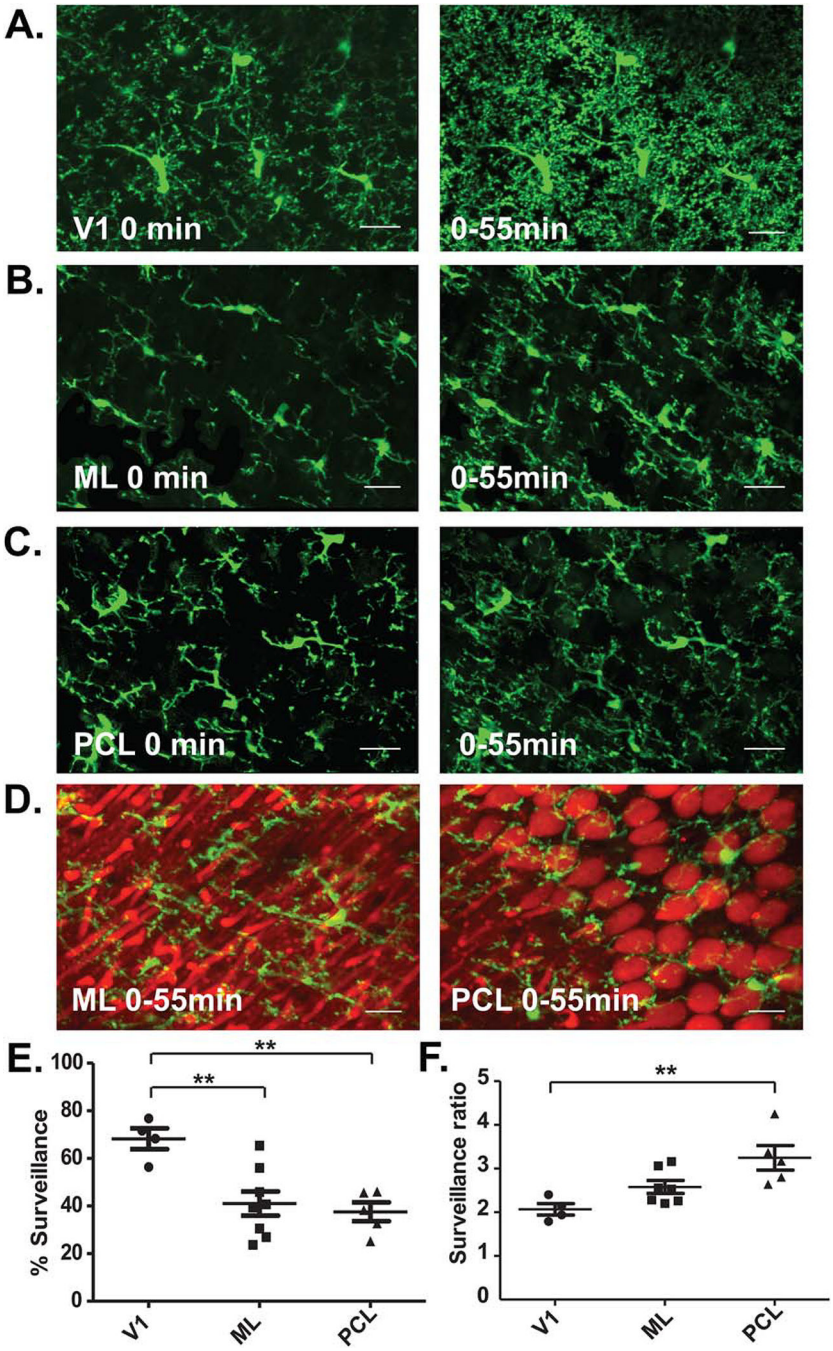


**Figure 4. Cerebellar microglia survey less of the parenchyma than cortical microglia**

(A-C.) *In vivo* images of microglia obtained in V1 (A.), and the ML (B.) and PCL (C.) of the Cb. Images shown are z-projections obtained at the first time point of imaging (leftmost panels) or an overlay of all imaging time points (rightmost panels). (D.) Examples of cerebellar microglial surveillance of Purkinje neuron dendrites (ML; left) and somas (PCL; right). (E.) V1 microglia effectively survey a large portion of the cortical parenchyma over the course of one hour. Cerebellar microglia in comparison effectively survey a significantly smaller portion of the cerebellar parenchyma (One-way ANOVA $F(2,14)=8.892$; $P<0.0032$.

Bonferroni *post hoc* V1 versus ML & PCL P<0.01 for both comparisons). (F.) When the % coverage over 1 hour is normalized to the coverage at the first time point we see that cerebellar microglia in the PCL survey the parenchyma more rapidly than visual cortical microglia (One-way ANOVA F(2,13)=7.604; P<0.0065. Bonferroni *post hoc* V1 versus PCL P<0.01). Scale bars =20μm.

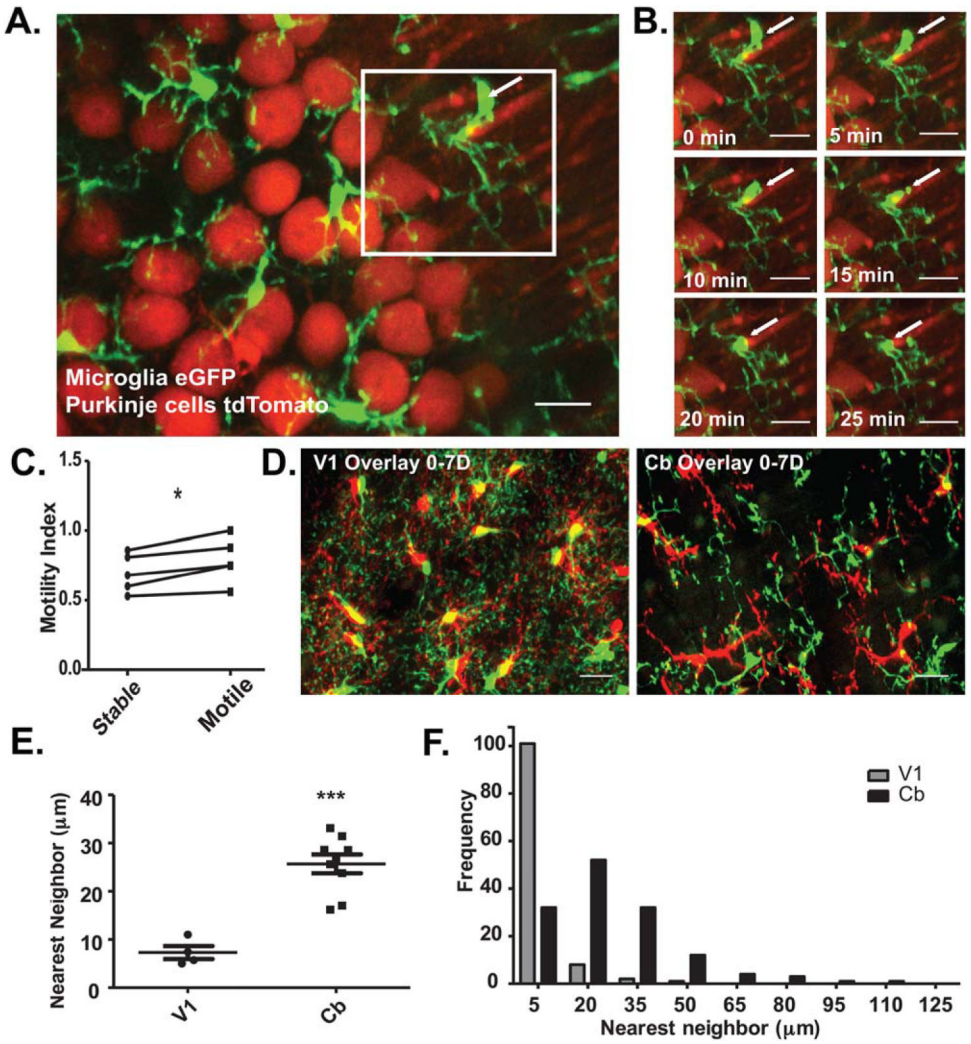


**Figure 5. Microglial cell bodies in the cerebellum exhibit motility**

(A.) An *in vivo* two-photon image showing Cb microglia (green) and Purkinje neurons (red). (B.) Time lapse of the boxed area in (A.) showing a microglial soma that migrates and alters its morphology. Within the course of 25 minutes the microglial soma moves ~10μm through the parenchyma (see arrow). (C.) Motility index of individual microglia in the same animalwith either stable or motile somas (paired t-test, $p<0.05$). (D.) Chronic imaging of microglia in V1 and Cb over 7 days. RGB overlays were created to show displacement of somas over this time frame - e red represents day 0, green represents day 7. Yellow indicates overlap. (E.) Quantification of the nearest neighbor distance between microglial locations on day 0 and day 7 in V1 and Cb. (Student's t-test $t(11)=5.898$, $p<0.0001$). (F.) Frequency distribution of the vector distance of the day 7 nearest neighbors to day 0 soma locations. Scale bars =20μm.

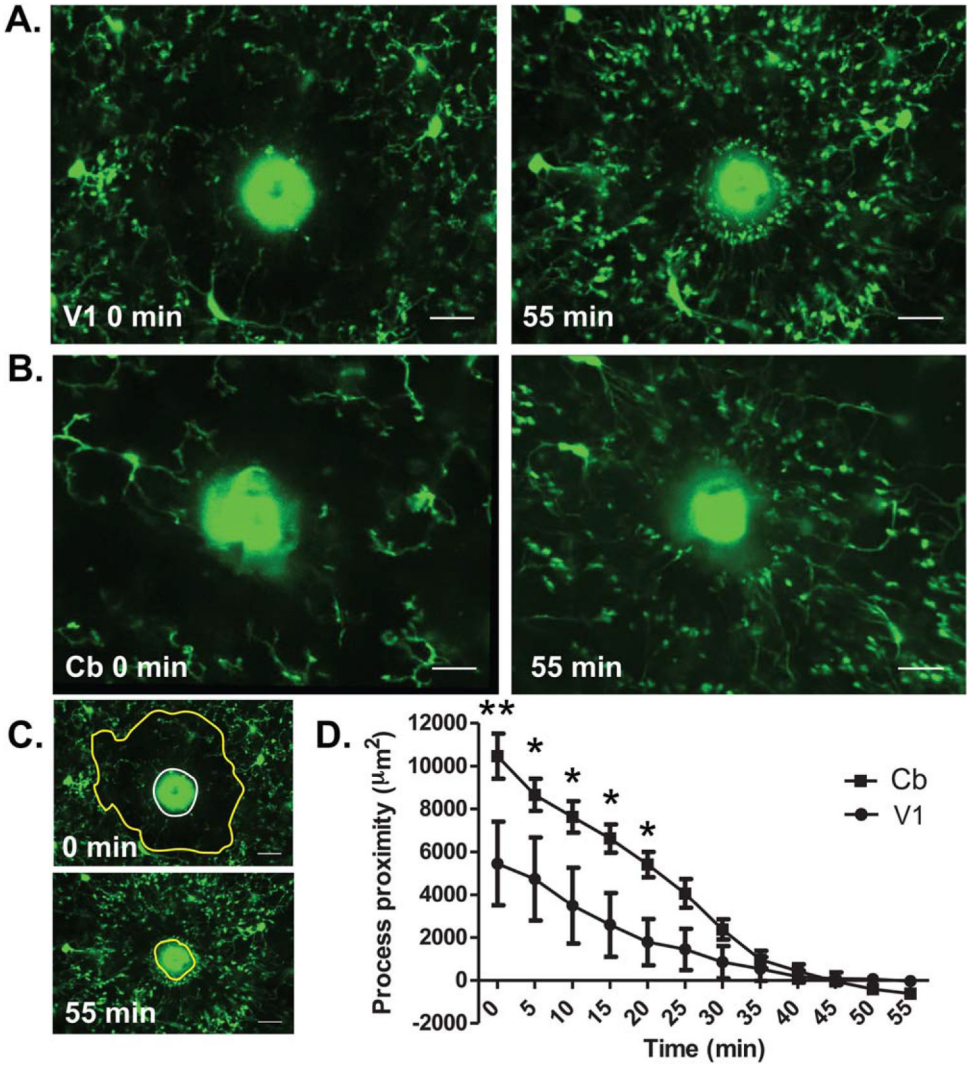


**Figure 6. Cerebellar microglia respond robustly to focal injury**

(A.) *In vivo* images of microglia in V1 at 0 minutes (left) and 55 minutes after laser ablation (right). (B.) *In vivo* images of cerebellar microglia at 0 minutes (left) and 55 minutes after laser ablation (right). (C.) Example of ablation analysis: the ablation core is selected out (white circle), and the border of the nearest microglial processes are measured at each time point as they migrate to the core (yellow). Cerebellar microglia are initially significantly further away from the ablation site, but by 30 minutes after injury have achieved the same proximity to the core of the injury as V1 microglia (Two-way repeated measures ANOVA $F(1,11)=6.096$; $P<.0001$ for interaction.) Scale bars =20μm.

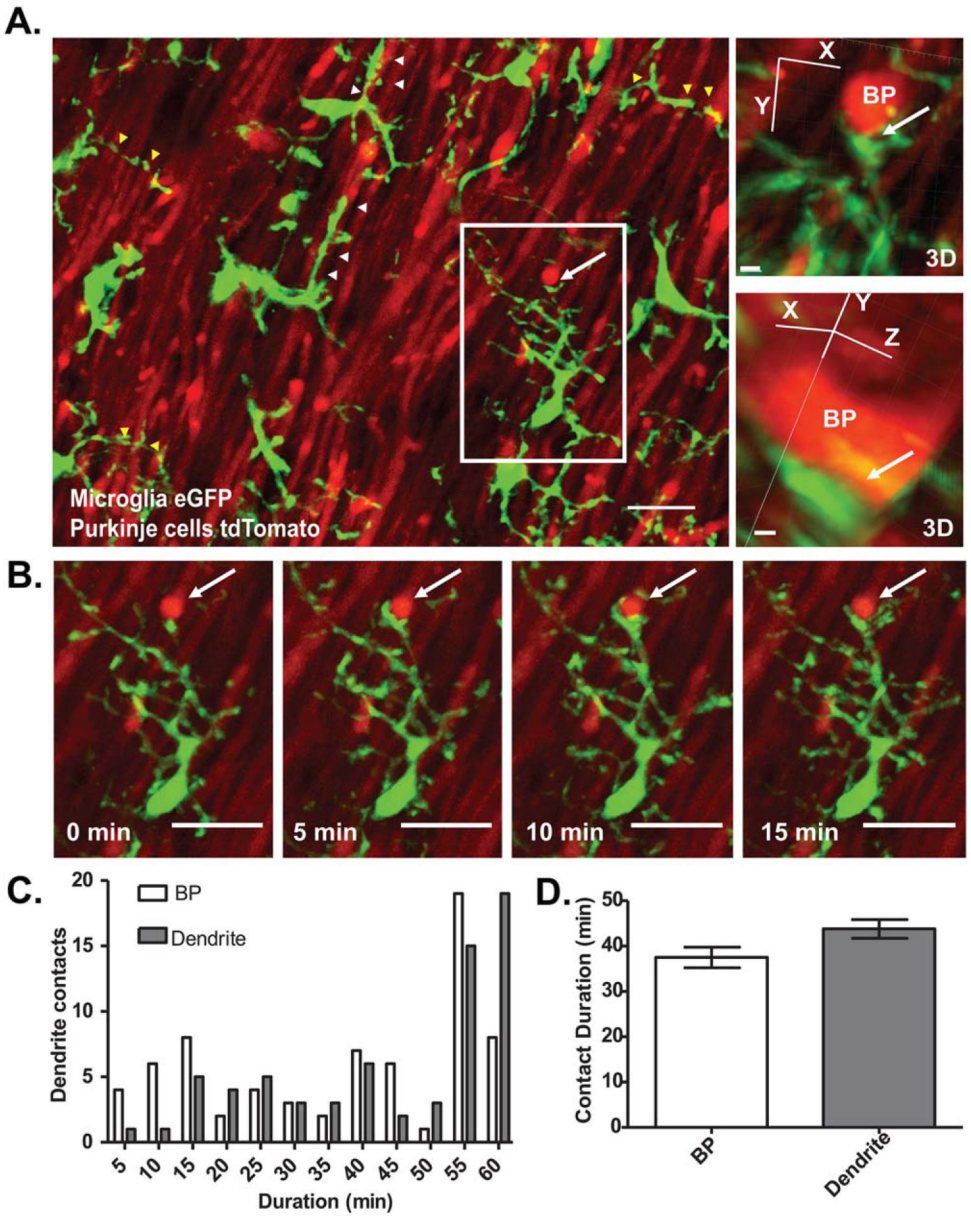


**Figure 7. Cerebellar microglia dynamically interact with Purkinje neuron dendrites**

(A.) *In vivo* image showing microglia (green) as they interact with Purkinje neuron dendrites (red). Notice that microglia extend their processes along the length of the dendrites (white arrowheads), wrap around dendrites (boxed region), and extend along many dendrites simultaneously (yellow arrowheads). The wrapping of processes around dendritic branch points is clearly visible in 3D reconstruction (right-most images) (B.) Over the course of 15 minutes an individual microglia cell (boxed region in (A.)) extends a process and makes a putative contact with a dendritic branch of a Purkinje neuron (arrow). (C.) A frequency distribution of the duration of microglial contacts with both dendrites and the branch points (BPs) of Purkinje neuron dendrites shows that there is high variability in the duration of microglia-neuron contacts (D.) There is no difference in the average contact duration of

microglial process with dendrites or BPs of dendrites. Scale bars =20μm for z-projections, and 3μm in 3D reconstructions.

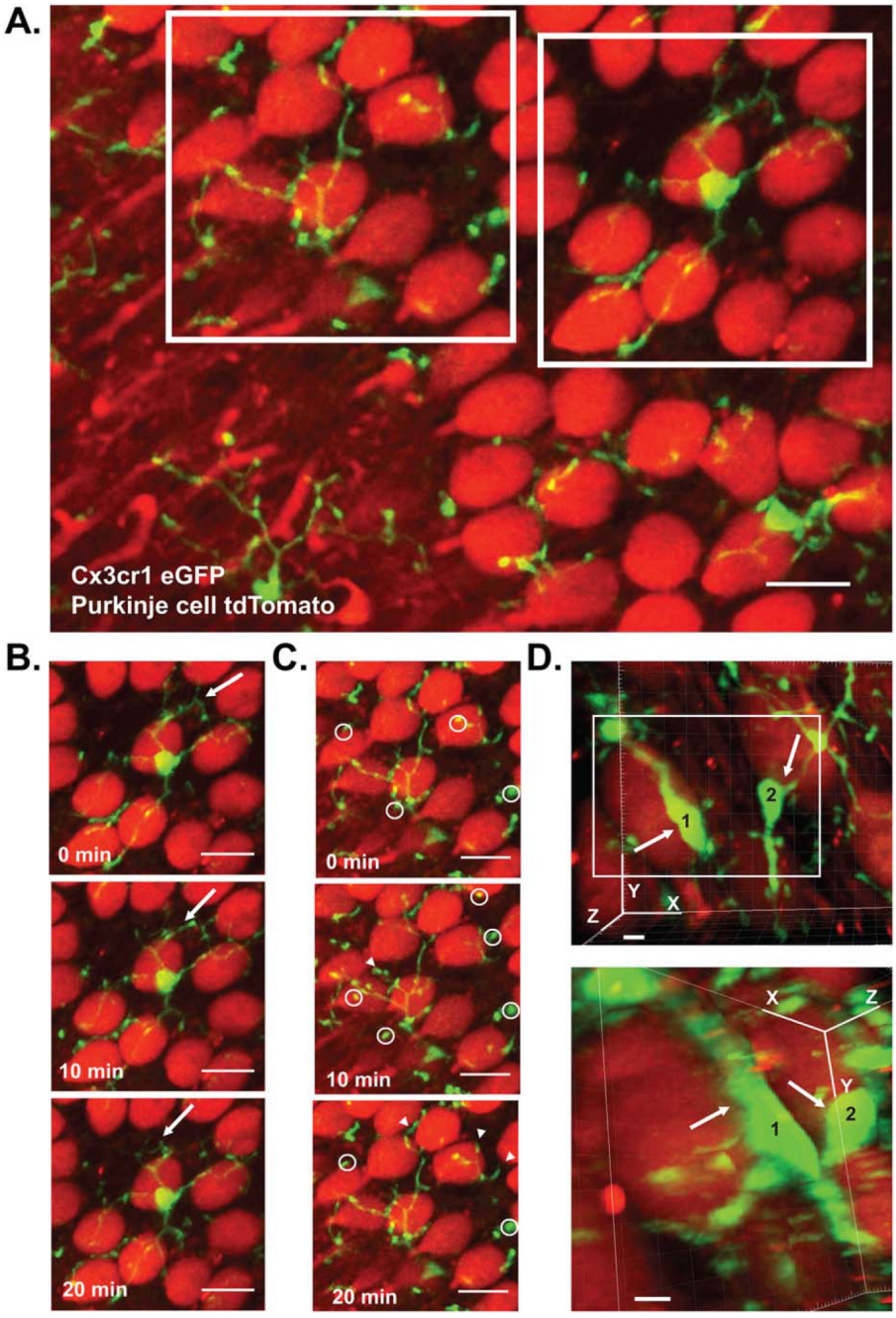


**Figure 8. Cerebellar microglia dynamically interact with Purkinje neuron somas**

(A.) *In vivo* image showing cerebellar microglia (green) that are interspersed amongst Purkinje neuron somas (red). (B.) A microglia cell (rightmost box in (A.)) interacting with multiple somas over the course of 20 minutes. The microglia also rapidly retracts some of its processes during surveillance, losing contact with the Purkinje neuron soma in the top right corner of the image (arrow) (C.) A second microglia (leftmost box in (A.)) extends numerous processes ending in bulbous pseudopodia (some examples of pseudopodia in circles) towards multiple Purkinje neuron somas, its processes elaborate and make extensive contacts over 30 minutes (arrowheads). (D.) 3D reconstruction of microglia contacting

Purkinje neurons. The contacts are shown from the top perspective (top image) as well as the side to show the close association of the microglia and neuron somas (bottom image). Scale bars =20μm for z-projections, and 5μm in 3D reconstructions.